Article

Not peer-reviewed version

Thermosensitive Hydrogel-Functionalized Mesoporous Silica Nanoparticles for Parenteral Application of Chemotherapeutics

Christina Voycheva , Marta Slavkova * , Teodora Popova , Diana Tzankova , Denitsa Stefanova , Virginia Tzankova , Ivelina Ivanova , Stanislav Tzankov , Ivanka Spassova , Daniela Kovacheva , Borislav Tzankov

Posted Date: 31 August 2023

doi: 10.20944/preprints202308.2153.v1

Keywords: Hydrogel gatekeeper; mesoporous silica nanoparticles; stimuli-sensitive delivery; chemotherapy; doxorubicin

Article

Thermosensitive Hydrogel-Functionalized Mesoporous Silica Nanoparticles for Parenteral Application of Chemotherapeutics

Christina Voycheva [1], Marta Slavkova [1,*] Teodora Popova [1], Diana Tzankova [5], Denitsa Stefanova [2], Virginia Tzankova [2], Ivelina Ivanova [3], Stanislav Tzankov [3], Ivanka Spassova [4], Daniela Kovacheva [4] and Borislav Tzankov [1]

[1] Medical University - Sofia, Faculty of Pharmacy, Department Pharmaceutical Technology and Biopharmacy, Sofia 1000, Bulgaria
[2] Medical University - Sofia, Faculty of Pharmacy, Department of Pharmacology, Pharmacotherapy and Toxicology, Sofia 1000, Bulgaria
[3] Medical University - Pleven, Faculty of Pharmacy, Pleven 5800, Bulgaria
[4] Institute of General and Inorganic Chemistry, Bulgarian Academy of Sciences, Sofia 1113, Bulgaria
[5] Medical University - Sofia, Faculty of Pharmacy, Department of Pharmaceutical Chemistry, Sofia 1000, Bulgaria
* Correspondence: mslavkova@pharmfac.mu-sofia.bg

Abstract: Hydrogels can offer many opportunities for drug delivery strategies. They can be used on their own or their benefits can be further exploited in combination with other nanocarriers. Intelligent hydrogels that react to changes in the surrounding environment can be utilized as gatekeepers and provide sustained on demand drug release. In this study, a hybrid nanosystem for temperature and pH sensitive delivery was prepared from MCM-41 nanoparticles grafted with newly synthesized thermosensitive hydrogel (MCM-41/AA-g-PnVCL). The initial particles were chemically modified by carboxyl groups attachment. Later, they were grafted with agar (AA) and vinylcaprolactam (VCL) by free radical polymerization. Doxorubicin was applied as a model hydrophilic chemotherapeutic drug. The successful formulation was confirmed by FT-IR and TGA. Transmission electron microscopy and dynamic light scattering analysis showed small particles with negative zeta potential. Their release behaviour was investigated in vitro in different pH media and at different temperatures. At tumor simulating conditions (40ºC and pH 4.0) doxorubicin was almost completely released within 72 hours. The biocompatibility of the proposed nanoparticles was demonstrated by in vitro haemolysis assay. These results suggest the possible parenteral application of the newly prepared hydrogel-functionalized mesoporous silica nanoparticles for temperature-sensitive and pH-triggered drug delivery at the tumor site.

Keywords: hydrogel gatekeeper; mesoporous silica nanoparticles; stimuli-sensitive delivery; chemotherapy; doxorubicin

1. Introduction

Conventional chemotherapy is a mainstaying treatment strategy for various cancer types [1]. It relies on the application of a variety of drug agents that can kill the cancerous cells. Unfortunately, their efficacy is usually hampered due to their inherent side effects on healthy tissues [2]. Another limitation is the need of frequent applications which causes immense burden to the patients' quality of life. Therefore, a significant trust and scientific effort has been put into the nanotechnological approach to overcome all the hurdles associated with chemotherapy. Various types of nanocarriers have been prepared and loaded with different chemotherapeutics aiming to achieve improved antitumor efficacy, prolonged and sustained release and to lessen the adverse events [3–8].

Hydrogels are a class of highly studied drug carriers with good biocompatibility and possibility to tune for desirable properties and different routes of administration [9]. Hydrogels exhibit a three-dimensional structure of interconnected and crosslinked polymers that can absorb extensive amounts of water and yet do not dissolve in water [10]. Recently, the attention has been directed towards the intelligent hydrogels. They possess stimuli-sensitive behaviour triggered by alterations in the

environmental conditions, such as temperature, pH, redox potential, light and others [11,12]. Amongst them the pH and thermo-sensitivity have been exploited a lot in the chemotherapy. This is mainly due to the fact that tumor cells are characterized with specific microenvironment with acidic medium and hyperthermia because of their intensive metabolism and vascularization [13]. Thus, a hydrogel with appropriate modifications can undergo reversible sol-gel transition at specific desired temperature and release the loaded drug [14]. Based on the temperature that causes the sol-gel transition the hydrogels can have either lower critical solution temperature (LCST) for hydrophilic to hydrophobic transition or upper critical solution temperature (UCST) for the opposite behaviour. In pharmaceutical application substances with LCST are widely used such as poly(N-isopropyl acrylamide) (PNIPAM), poly(N-vinylcaprolactam) (PVCL), poly(N-vinylalkylamide), poly(2-hydroxyethylmethacrylate) (PHEMA), Pluronic, chitosan, hyaluronic acid, etc. [15]. The specific temperature causing the on demand drug release can be finely tuned by chemical or physical modifications of the parent polymer [14]. Nevertheless, there are some challenges in the application of hydrogels in chemotherapy such as lower mechanical strength and troublesome sustained release especially for hydrophilic drugs [16,17].

Developing composite systems for drug delivery has been shown to surmount the limitations of either one of their components on its own [18]. Those are hybrid nanocarriers that combine the properties of different carriers, i.e. hydrogel and inorganic nanoparticles [19]. Different examples of their combinations can be found in the literature [20–22]. Thermosensitive hydrogels have been used by other researchers as gatekeepers to achieve sustained and specific drug delivery [15,23]. A very suitable inorganic nanocarrier to be functionalized with appropriate hydrogel gatekeeper are mesoporous silica nanoparticles (MSNs) [18,24]. MSNs are characterized with high specific surface area, adjustable pore size, high hydrothermal stability, large pore volume, biocompatibility and very low toxicity [18,25–28]. Moreover, their internal and external surface is highly covered with silanol groups which can easily undergo functionalization [28]. The introduction of new chemical modalities (such as carboxylic groups) could be further utilized as a site for grafting with polymers, i.e. hydrogels [29].

The natural polymers are very attractive for modifications because of their nontoxicity and biodegradability. The marine polysaccharides are extracted from renewable sources and cost-effective [30]. Agar is a polysaccharide derived from algae which can form a strong biocompatible hydrogel. As an excipient it is widely used in the pharmaceutical practice in the role of a binder, filler, thickening agent, gelling agent, etc. [30,31]. Agar on its own does not possess thermo-sensitive properties, but can easily be modified by suitable grafting and result in a thermoresponsive hydrogel [32]. Therefore, agar was selected as a backbone for the gatekeeper modification of MSNs in the current study.

The present research aims at obtaining hydrogel-functionalized mesoporous silica nanoparticles for thermo-sensitive drug delivery. Doxorubicin was selected as a model drug due to its hydrophilic nature and versatile application in many forms of solid tumours and leukaemia [33]. It was hypothesized that the hybrid nanoparticles could be a suitable candidate for parenteral chemotherapy. The biocompatibility of the proposed nanocarrier was evaluated through its haemolytic potential.

2. Results and Discussion

The novel hydrogel AA-g-PnVCL was synthesized using a free radical initiated polymerization in nitrogen atmosphere as the amount of monomer and radical initiator concentration were chosen based on previous work. The rationale for the chosen ratios lies into the LCST (40 ºC) of the obtained polymer together with sufficient grafting efficiency (62.4%) [34].

2.1. Synthesis of Hydrogel-Functionalized Nanoparticles MCM-41/AA-g-PnVCL

Here, a two-step-controlled grafting is proposed. First functionalization (carboxylation) of the mesopores and surface of MCM-41 was performed, followed by free radical polymerization of AA and nVCL in the presence of carboxyl modified MCM-41, using 2,2'-Azobis(2,4-dimethylvaleronitrile) (AMVN) as a free radical initiator (Figure 1). The carboxymodification of MCM-41 was carried out to provide reactive sites for attaching AA-g-PnVCL.

Preprints (www.preprints.org) | NOT PEER-REVIEWED | Posted: 31 August 2023 doi:10.20944/preprints202308.2153.v1

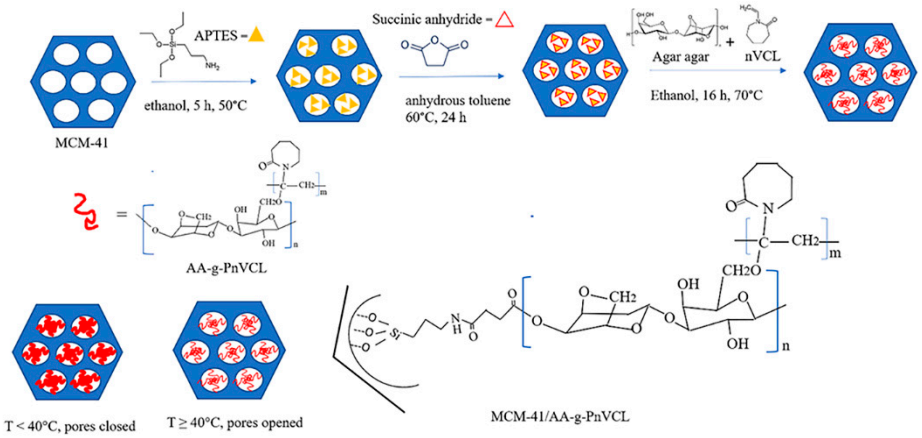

Figure 1. Synthesis of the hydrogel-functionalized silica nanoparticles.

2.2. Characterization of the AA-g-PnVCL and MCM-41/AA-g-PnVCL

2.2.1. FT-IR

The FT-IR spectra of all samples are presented on Figure 2. The parent silica MCM-41 materials were characterized by an intensive band at 1042 cm-1 which was due to the asymmetric stretching vibration of silica structure (Si–O–Si), also the band at 962 cm–1 was corresponding to the stretching vibrations of surface Si–O groups [35,36]. After Dox loading onto MCM-41 no shifting of silanol group bands is observed. It can be assumed that Dox is physically entrapped in the nanocarriers. The significant shifting of silanol group bands to 1069 cm−1 and 946 cm−1 and the appearance of the stretching vibration of carboxylic groups at 1552, 1622 and 1728 cm−1 show the successful attachment of COOH to the MCM-41 [37].

The shifting of the characteristic band of hydroxyl groups to 3382 cm-1 and the disappearance of the CH2OH band visible at 1065 cm-1 in the spectrum of AA-g-PnVCL are evidence of the successful grafting of AA-g-PnVCL on MCM-41-COOH. Doxorubicin shows stretching vibrations of O-H and N-H bonds in the range 3300-3550 cm-1. The pick at 1730 cm-1 correlates with COOH groups, while these at 1615 cm-1 and 1580 cm-1 with the ring (phenol), 1524 cm-1 with aromatic ring (C=C), 1412 cm-1 (N-H), 1282 cm-1 (C-C), 1233 cm-1 (C-N) and 993 cm-1 (C-OH) and were confirmed with literature data [38].

The spectrum of Dox loaded on the hybrid MCM-41/AA-g-PnVCL nanoparticles shows only a lowering of the intensities, but no significant shifting in the characteristic peaks. This fact suggests that Doxorubicin was physically included in the MCM-41/AA-g-PnVCL particles.

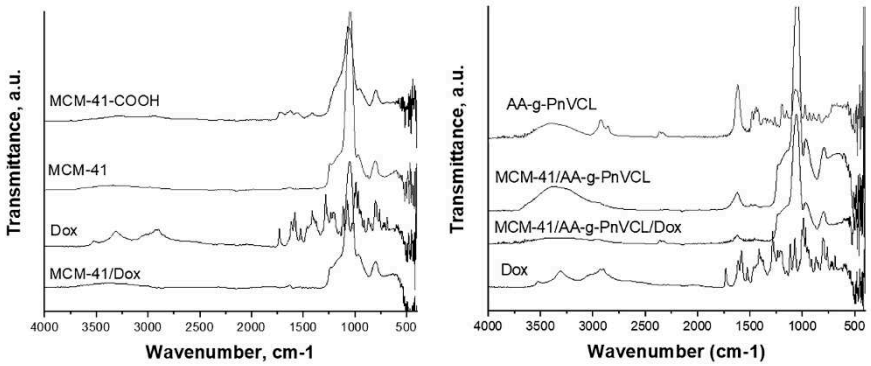

Figure 2. FT-IR spectra of Dox, the parent MCM-41, Dox loaded MCM-41, carboxyl modified MCM-41, AA-g-PnVCL, MCM-41/AA-g-PnVCL and loaded hydrogel-functionalized nanoparticles.

2.2.2. TEM

TEM studies were performed for analysis of the size and structure of MCM-41 and MCM-41/AA-g-PnVCL (Figure 3). As seen, MCM–41 has an expected porous structure (Figure 3 a). The same

Preprints (www.preprints.org) | NOT PEER-REVIEWED | Posted: 31 August 2023 doi:10.20944/preprints202308.2153.v1

structure is observed for the MCM-41/AA-g-PnVCL as well (Figure 3 b). The hydrogel on the surface of silica particles did not influence significantly the morphology of MCM-41. The darker areas represent silica particles and lighter areas correspond to the hydrogel crown formed around the MCM-41surface due to grafting with AA-g-PnVCL (Figure 3b).

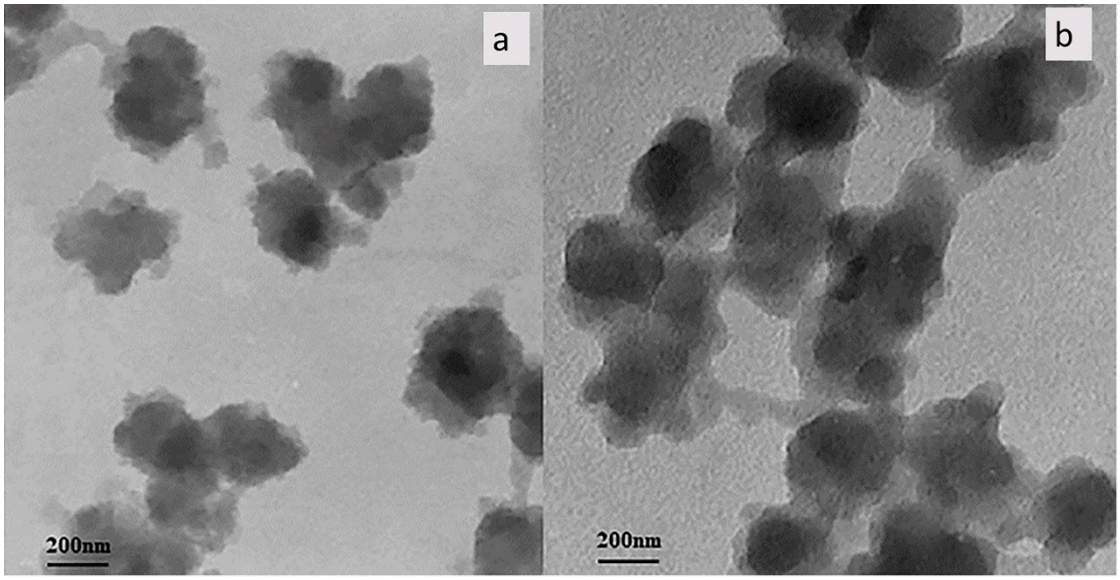

Figure 3. Transmission electron micrographs of MCM-41 (a) and MCM-41/AA-g-PnVCL (b).

2.2.3. TGA

The attachment of AA-g-PnVCL on MCM-41 particles could be evidenced by the thermogravimetric analyses shown in Figure 4. It presents TG curves of MCM-41, hydrogel AA-g-PnVCL and the hybrid system MCM-41/AA-g-PnVCL in a temperature range 25–700oC. Three main thermal steps are registered for the hydrogel.

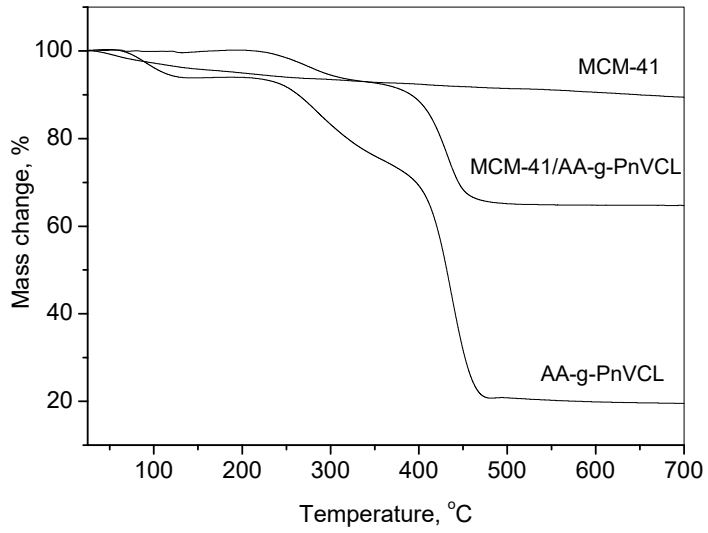

Figure 4. TG-curves of MCM-41 and MCM-41/AA-g-PnVCL and AA-g-PnVCL.

The first temperature weight loss ranges from 60°C to about 120°C, where the polymer loses about 8 % mass, due to dehydration. The second step is from 205°C to 340°C due to the depolymerization of the agar-agar, with a weight loss of about 25% of its mass. The third decomposition step occurs from about 340°C to nearly 475°C, where 35% of the material's mass is lost probably due to the degradation of nVCL units with full mass loss of nearly 80%. One could observe that the pure MCM-41 particles possess gradual and slight weight loss in the whole temperature

Preprints (www.preprints.org) | NOT PEER-REVIEWED | Posted: 31 August 2023 doi:10.20944/preprints202308.2153.v1

range (10%), while the thermal decomposition stages of MCM-41/AA-g-PnVCL appear at the same stages and temperatures as AA-g-PnVCL and the difference between the mass loss of MCM-41 and MCM-41/AA-g-PnVCL is about 25%. Hence, there is a successful attachment of the AA-g-PnVCL on the MCM-41 particles.

2.2.4. XRD

Small-angle part of the XRD patterns of MCM-41 and MCM-41/AA-g-PnVCL and MCM-41/AA-g-PnVCL/Dox are presented in Figure 5. X-ray Powder Diffraction Pattern of the MCM-41 material exhibits four pronounced peaks - the most intense (100) and well-split (110) and (200) along with (210) reflections as an indication of hexagonal pore structure with a high degree of ordering. The unit cell parameter is 46.79(5) Å. The pattern of the MCM-41/AA-g-PnVCL shows the slight shift of the peaks towards higher degrees 2 theta and peak asymmetry which could be attributed to the changes of the pore wall thickness due to the attachment of the AA-g-PnVCL on MCM-41. The pattern of the MCM-41/AA-g-PnVCL/Dox shows only one peak with low intensity indicative for successful preparation of the finally loaded material.

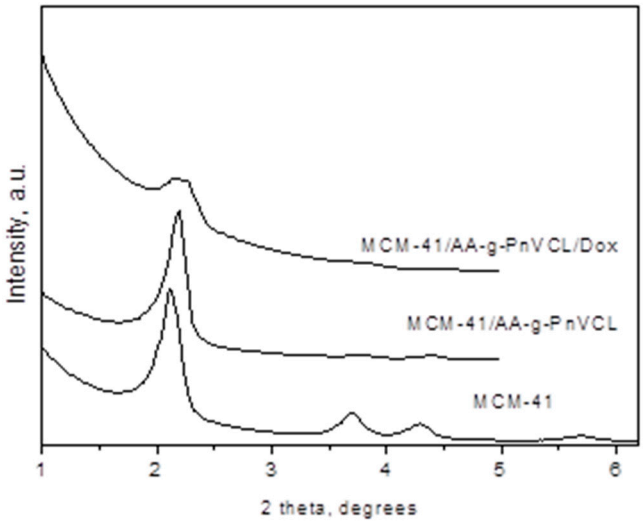

Figure 5. Small angle part of the XRD patterns of MCM-41 and MCM-41/AA-g-PnVCL and MCM-41/AA-g-PnVCL/Dox.

2.2.5. Temperature- Sensitive Behavior

AA has no temperature sensitivity, while the LCST of PnVCL is around 32-33°C but it is lower than the normal body temperature. Therefore, each of the components on their own does not provide sufficient thermoresponsive properties. By grafting nVCL units on the AA hydrophilic backbone thermosensitivity is achieved. The change in the ratio of the hydrophilic polymer and hydrophobic monomer gives different temperature behavior of the polymers. The synthesized polymer AA-g-PnVCL (Figure 6 a) at a predetermined ratio of the components has the characteristics necessary for the subsequent work with doxorubicin loading and achieving smart release at the temperature of 40°C [34]. Thermoresponsive polymers have a homogenous aqueous solution below LCST and undergo heterogeneous disperse system change above it. They prevent the release of the drug before LCST is reached and provoke delivery of the active substance above LCST in larger quantities when the utility is the largest. The sharp changes from a swollen to a collapsed state are an opportunity to use this hydrogel as gatekeeper and release the anti-cancer drug in a smart temperature-sensitive manner.

Preprints (www.preprints.org) | NOT PEER-REVIEWED | Posted: 31 August 2023 doi:10.20944/preprints202308.2153.v1

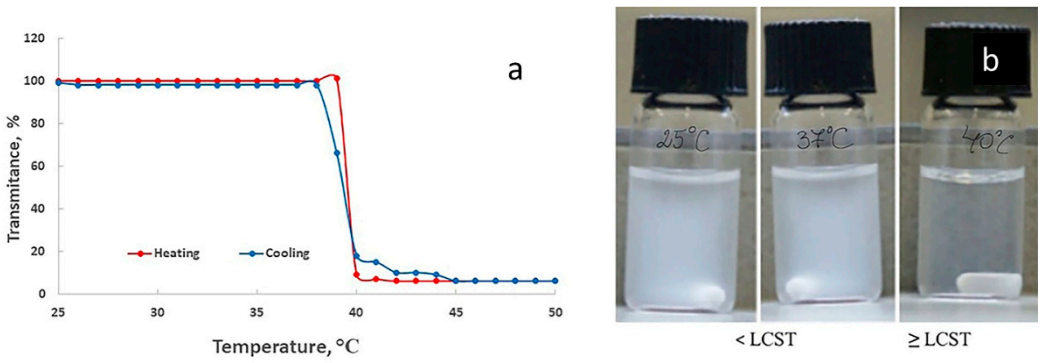

Figure 6. a) LCST of AA-g-PnVCL and thermoresponsive behavior of hydrogel-functionalized nanoparticles in diluted aqueous dispersion (4 mg/mL); b) macroscopic photos of the corresponding dispersion at various temperatures.

The grafting of MCM-41 nanoparticles with the synthesized thermo-sensitive hydrogel with an LCST value higher than usual body temperature could keep the API in the mesopores, preventing or drastically slowing its release below a certain temperature and hastening it if the local temperature is above the polymer LCST. The thermoresponsive behavior of hybrid nanoparticles is evident in Figure 6 b. The drug release can be provoked by applying exterior heat in the field with tumor tissue or using the natural difference between healthy and tumor tissues known as local tumor hyperemia [39].

2.2.6. Dynamic Light Scattering (DLS)

Pristine MCM-41 nanoparticles are characterized with small particle size and negative zeta potential which is in accordance with literature data [40,41]. The negative charge is due to the presence of silanol groups on their surface which undergo deprotonation n aqueous medium. Measurements performed by DLS analysis show increased particle size and polydispersity index after polymer grafting on the surface of the MCM-41 particles and negative z-potential above 20 mV (Table 1). The engagement of surface silanol groups in the grafting with the thermosensitive polymer leads to a decrease in the absolute value of zeta potential. Similar results after grafting are reported by other publications [40]. The value of the polydispersity index (PDI) shows the stability of parent particles and size distribution within narrow limits. The polymer grafting affects predominantly the surface of carboxyl modified MCM-41 as can be seen from TEM images as well (Figure 3B). Therefore, an increase in particle size is observed as can be expected due to the attached polymer chains. The increase of the PDI after preparation could be explained with the different number of grafted polymer molecules on each MCM-41-COOH particle. The decrease in the absolute zeta potential value can also be a reason for particle aggregation and increased polydispersity. After Dox loading, the PDI and size of the particles are maintained in the same range as the ones of the Dox-free hybrid nanoparticles. These results suggest that Dox doesn't affect the size of the prepared hybrid nanoparticles and no significant change is observed in their particle size distribution. The decrease in the absolute value of the zeta potential could be due to electrostatic interaction between the nanocarrier and Dox. It is well known that Dox is a cationic drug (pKa=8.3) which is positively charged in physiological conditions due to the presence of amine groups [42,43]. The results for the average size are in agreement with the TEM analysis.

Table 1. Average size, polydispersity index (PDI) and zeta potential results from DLS analysis.

Parameter	MCM-41	MCM-41/AA-g-PnVCL	MCM-41/AA-g-PnVCL/Dox
Size, nm	217 ± 7.3	360 ± 8.4	369 ± 3.3
PDI	0.31	0.86	0.83
Zeta potential, mV	- 37.1 ± 3.7	- 26.6 ± 3.6	- 19.8 ± 2.4

2.2.7. Dox Loading Efficiency

Post-surface grafting API loading was chosen in the present study. Based on literature data it is suggested that during the numerous steps of grafting and extraction, Dox can be lost from the

Preprints (www.preprints.org) | NOT PEER-REVIEWED | Posted: 31 August 2023 doi:10.20944/preprints202308.2153.v1

nanocarriers [44]. Dox loading onto unmodified MCM-41 was found to be 49 % while loading efficiency on MCM-41/AA-g-PnVCL was calculated to be 59 %. It can be expected that the active substance is physically encapsulated in the grafted MCM-41 particles based on the results from IR spectroscopy. The higher loading capacity of the hybrid particles is probably due to the formation of internal free volumes from the chains of AA-g-PnVCL attached to the surface of MCM-41.

2.2.8. Drug Release

The expected temperature and pH dependent release of Dox was monitored by performing in vitro dissolution test in pH 7.4 and 4.0 buffer medium at 25°C, 37°C and 40°C, corresponding to the room, normal body temperature and tumour hyperemia. The results are presented on Figures 7 and 8.

Doxorubicin release from non-modified MCM-41/Dox at pH 7.4 is slow (around 25 % within the first 6 h of the study, Figure 7 a). At pH 7.4 Dox molecules are partially protonated as can be expected based on their pKa=8.22 [43,44]. Therefore, at this pH Dox is positively charged while the MSN carrier's silanol groups are characterized with negative charge. This leads to electrostatic attraction between the carrier and the API and the drug is retained. These results are in accordance with other studies [39–42]. On the 72nd hour in pH 7.4 (Figure 8 a), regardless of the temperature, about 40% were released from nonmodified particles. This suggests incomplete but still sufficient Dox release at normal physiological conditions which could cause toxic systemic effects.

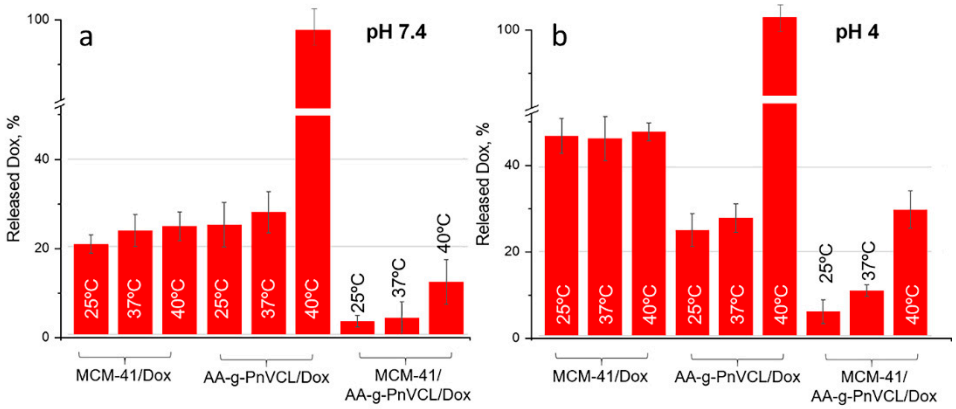

Figure 7. Released Doxorubicin amount (%) at 6th hour during an in vitro dissolution test at pH 7.4 (a) and pH 4.0 (b) at different temperatures (25; 37; 40ºC); n = 3 ± SD.

At the same time the thermosensitive AA-g-PnVCL/Dox shows complete release of Dox at pH 7.4 but only at 40º C (Figure 7 a). The results obtained from the in vitro dissolution test at 25°C and 37°C showed a delayed release in the initial phase as well as a slow release over time. Lower than 5% of the active substance was released in the first 6 hours followed by about 15% released by the 72nd hour (Figure 8 a). This delay in the release is expected due to the swollen state of the hydrogel at room temperature and the normal body temperature. This suggests the possibility for temperature sensitive drug delivery at the tumor site as shown in literature [34]. About 10% Dox release from the hybrid nanoparticles at pH 7.4 and 40°C was reported at the 6th hour (Figure 7 a) and about 25 % at the 72nd hour (Figure 8 a). This temperature is above the LCST and the hydrogel on the surface of the particles is in its collapsed state, which allows the opening of the pores and the release of the drug from the inside. The hydrogel acts as a gatekeeper and Dox is released only after the required conditions are met. There is statistically significant difference in the released Dox amount from MCM-41/AA-gPnVCL at the three investigated temperatures ($p < 0.05$) suggesting that the thermosensitive release is maintained in the preparation of hybrid nanoparticles.

Preprints (www.preprints.org) | NOT PEER-REVIEWED | Posted: 31 August 2023 doi:10.20944/preprints202308.2153.v1

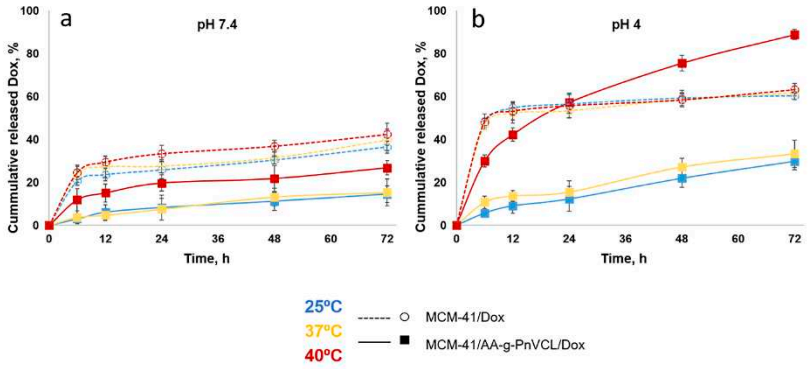

Figure 8. Release profiles of doxorubicin from MCM-41/AA-g-PnVCL and MCM-41 nanoparticles in a buffer medium with a pH of 7.4 (a) and pH of 4 (b) at different temperatures (25; 37; 40ºC); n = 3 ± SD.

At pH 4.0 (Figure 7 b and Figure 8 b) all of the investigated nanocarriers exhibit increased Dox release which can be expected due to its known better solubility in acidic medium [45,46]. Such acidic conditions are expected for the tumor cells because of their extensive metabolism [47]. The pristine MCM-41 loaded with Dox at pH=4.0, present significant release with some burst effect in the first 6 h of the dissolution with no temperature sensitivity ($p = 0.8$). Therefore, no actual sustained release is observed. In the acidic medium the thermosensitive hydrogel AA-g-PnVCL loaded with Dox again completely released the API within 6 h at 40ºC (Figure 7 b). At temperatures lower than LCST a sustained release is observed with significantly lower Dox amount being released from the thermopolymer ($p < 0.05$).

Comparing the release of Dox at 6 h in pH 4.0 from MCM-41, AA-g-PnVCL and MCM-41/AA-g-PnVCL (Figure 7 b), sustained and temperature-triggered release is observed from the hybrid nanoparticles. The newly prepared hybrid nanoparticles at the simulated tumor conditions (pH = 4 and 40ºC) show sustained release without burst effect in the initial phase (Figure 7 b). Over time gradual controlled release is observed and nearly 90% of released API is achieved within 72 h (Figure 8 b). This could lead to the assumption that no fluctuation in the Dox concentration at the target site will be present. These findings support the expectations that combining two types of delivery systems, i.e. thermo-sensitive hydrogel and MSNs, leads to a superior properties and could improve the anticancer therapy.

Based on the data obtained, it can be assumed that the modification of MCM-41 particles with a thermopolymer allows a delayed and stimuli triggered release compared to the hydrogel alone and unmodified particles. Providing very low drug release at a physiological pH of 7.4 at 37°C is a prerequisite for lowering the systemic toxicity of the novel MCM-41-AA-gPnVCL nanoparticles. Sustained and almost complete release from the hybrid nanoparticles is observed only when an area with local tumor hyperemia and acidic pH is reached.

2.2.9. Hemolysis Assay

The hemolytic assay is a widely used primary screening method for in vitro biocompatibility testing of new drug substances. The hemolytic activity of the tested compounds was compared with the effects of Triton X-100 as shown in Figure 9. Triton X-100 induced complete hemolysis (by 100% vs control) after 1h incubation. The highest concentrations of free Dox (10.87 μg/ml) were found to induce a hemolysis by 8 % vs untreated control. In contrast, at the same concentrations Dox loaded in nanoparticles (MCM-41-Dox, AA-g-PnVCL-Dox and MCM-41/AA-g-PnVCL) did not show hemolytic effect, since the rate of hemolysis was lower than 5% (respectively, 1.6 %, 3.3 % and 1.8 % vs untreated control).

Preprints (www.preprints.org) | NOT PEER-REVIEWED | Posted: 31 August 2023 doi:10.20944/preprints202308.2153.v1

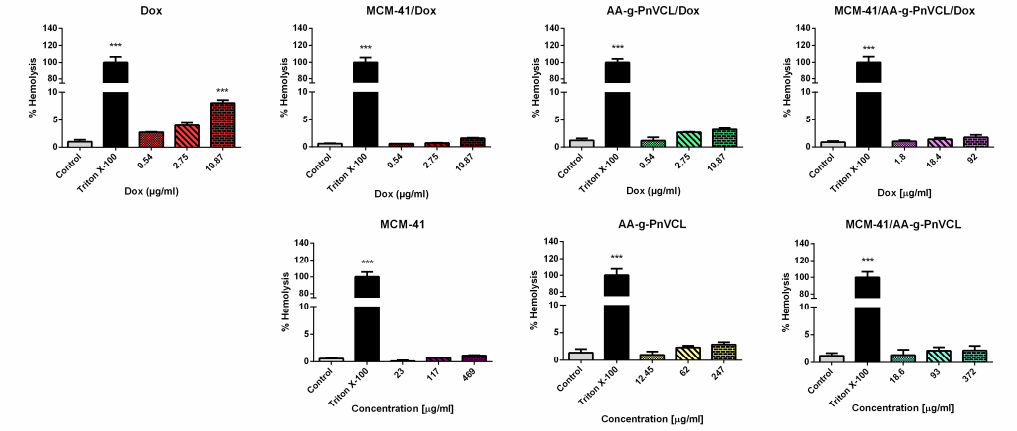

Figure 9. Hemolytic effects of free Dox; Dox loaded in MCM-41; Dox loaded in AA-g-PnVCL; Dox loaded in MCM-41/AA-g-PnVCL; MCM-41; AA-g-PnVCL; MCM41/AA-g-PnVCL on human erythrocytes. The results are expressed as means ± SD of triplicate assays (n=3). All groups were compared statistically vs untreated controls by one-way Anova with Dunnet's post-test ***p <0.001 vs control.

Empty nanoparticles and Dox loaded in MCM-41, AA-g-PnVCL and MCM-41/AA-g-PnVCL did not show significant hemolytic effects. Our results are in accordance with the study of Saroj et al., who reported that pH-sensitive poly acrylic acid functionalized MCM-41 nanoparticles demonstrated hemocompatibility similar to negative control group [48]. Zhao et al. reported good biocompatibility with human erythrocytes of mesoporous silica nanoparticles MCM-41, compared to the highly hemolytic amorphous silica [49].

Thus, the results from our experiments confirmed good hemocompatibility of the empty carriers which is a promising perspective for parenteral application. Interestingly, we found, that the loading of Dox in MCM-41, AA-g-PnVCL and MCM-41/AA-g-PnVCL nanoparticles improved its hemocompatibility compared to the effects of free Dox.

3. Conclusions

A hybrid controlled drug delivery system based on AA grafted with PnVCL and attached to the surface of MCM-41 was obtained successfully. The newly synthesized hydrogel could efficiently serve as a gatekeeper on the MSNs governing the drug release in response to the environmental temperature and pH. The model drug doxorubicin was almost completely released only in the simulated cancer tissue conditions (40 ºC and pH=4.0). In addition, the hydrogel to the surface of the silica particles form internal cavities for drug molecules which allows a high loading efficiency (59%). The release profile was prolonged within 72 h time frame which could limit the frequency of treatment. The hemolysis assay demonstrated good biocompatibility of empty and Dox-loaded nanoparticles since no significant hemolysis of red blood cells was observed.

All presented results suggest that the developed hydrogel-functionalized MCM-41/AA-g-PnVCL-based platform is an attractive candidate for stimuli-triggered and controlled drug release for chemotherapeutic agents. Once the preparation, successful "smart" release properties and safety upon parenteral application are proven further studies would be necessary to evaluate its therapeutic efficacy in vitro and in vivo.

4. Materials and Methods

4.1. Materials

MCM-41, 3-aminopropyltriethoxysilane (APTES), succinic anhydride, anhydrous toluene, agar-agar powder and N-vinyl caprolactam (nVCL) were purchased from Sigma Aldrich (USA). 2,2'-Azobis(2,4-dimethylvaleronitrile) (AMVN) and Hydroquinone were purchased from TCI America. Ethanol, Disodiumhydrogen phosphate dihydrate and Potassium dihydrogen phosphate were all purchased from Merck (Darmstadt, Germany). Deionized water was obtained by ion exchange.

 doi:10.20944/preprints202308.2153.v1

4.2. Synthesis of Hydrogel-Functionalized MCM-41 Nanoparticles

4.2.1. Synthesis of COOH Modified MCM-41 Particles (MCM-41-COOH)

The carboxylation of MCM-41 was carried out in two steps. The first one included intermediate amination in which MSNs and 3-aminopropyltriethoxysilane (APTES) were mixed in ethanol for 5 hours at 50°C. Then, a two-step washing was conducted firstly with ethanol and thereafter with deionized water. The resulting particles were dried at room temperature followed by azeotropic dehydration. They were placed in toluene at 115°C and the adsorbed water was removed.

The second step was the carboxylation of the amino-functionalized MCM-41. For this purpose, succinic anhydride (6.6 mmol) was added to the dispersion of the amino-modified MCM-41 in anhydrous toluene at 60°C for 24 h. Carboxylation was performed assuming MCM-41 were pre-functionalized with 2 wt% amino content. The resulting modified particles were dried for 6 h by vacuum evaporation at 25°C temperature and the obtained MCM-41-COOH were used for further thermopolymer attachment.

4.2.2. Synthesis of MCM-41-COOH/AA-g-PnVCL Nanoparticles

The formation of hydrogel containing AA to nVCL in molar ratio 20:1 in the presence of AMVN as an initiator (AMVN: nVCL in molar ratio 1:20) by free radical polymerization technique is explained elsewhere [34]. To obtain the hybrid nanosystem a modified polymerization method was applied according to the following procedure: AA (20 mg) was dissolved in 40 ml of distilled water at 90°C with constant stirring. MCM-41-COOH particles (250 mg) were homogeneously dispersed in the AA solution. Further, nVCL (140 mg) was dissolved in 40 ml of 95% ethanol and added to the mixture in a three-neck round bottom flask in nitrogen atmosphere for 60 minutes. Next, a solution of AMVN in 20 ml 95% ethanol was added and nitrogen flow continued for another 15 minutes before closing the flask. The reaction continued with ongoing stirring in a thermostatic paraffin bath (70°C) for 16 h. Finally, the grafting procedure was terminated by adding a saturated solution of hydroquinone. The resulting MCM-41/AA-g-PnVCL particles were precipitated in acetone and separated by centrifugation (15 000 rpm). Removal of the homopolymer (PnVCL) was carried out by extraction with 95% ethanol for 24 h. Then the MCM-41/AA-g-PnVCL were dried under vacuum to constant weight and further subjected to characterization. A schematic representation of the procedure is shown on Figure 1.

4.3. Characterization of the Hydrogel, MCM-41 Nanoparticles and Hydrogel-Functionalized Nanoparticles (MCM-41/AA-g-PnVCL)

4.3.1. Transform Infrared Spectroscopy (FTIR)

Thermo-Nicolet FTIR instrument equipped with an attenuated total reflectance (ATR) device (Thermo scientific Nicolet) was used to collect IR spectra in the range of 4000–400 cm-1 and with a resolution of 4 cm-1 for the free components as well as the grafted products.

4.3.2. Transmission Electron Microscopy (TEM)

The size and structure of the gatekeeper-modified nanoparticles were characterized using transmission electron microscopy (JEOL JEM 2100 h STEM (200 kV; point-resolution 0.23 nm)).

4.3.3. Thermogravimetric Analysis (TGA)

PerkinElmer TGA4000 thermogravimeter was used to perform TGA and operating conditions were as follows: argon gas at 60 ml/min, temperature range from 40°C to 820°C with a heating rate of 10°C/min. Specialized software Pyris v.11.0.0.0449 was used for data collection and processing.

4.3.4. X-ray Powder Diffraction (XRD)

XRD measurements were applied to characterize the nanoparticle crystallographic structure. Small-angle parts of the XRD patterns were collected from 0.3 to 8° 2θ using a knife-edge anti-scatter screen attachment of the primary beam. patterns on Bruker D8 Advance diffractometer with Cu Kα radiation and LynxEye detector.

 doi:10.20944/preprints202308.2153.v1

4.3.5. Lower Critical Solution Temperature (LCST) Determination

The characterization was performed via transmittance measurements on a UV Spectrophotometer (Thermo Scientific Evolution 300, USA) at 500 nm with a heating/cooling cycle step 1°C after incubating the samples for 5 minutes at each temperature. The light passed through the solution and the transmittance in % was measured. At LCST a change in turbidity of the AA-g-PnVCL solution occurs.

4.3.6. Dynamic Light Scattering (DLS)

Nanoparticle size, polydispersity index, and zeta potential were determined using a Zetasizer (Zetasizer Nano ZS, Malvern Instruments, Worcestershire, UK). The samples (0.1% w/v) were dispersed in distilled water, sonicated for 20 minutes and measured at a scattering angle of 90o and at 25o C.

4.3.7. Drug Loading and Loading Efficiency

The wet mixing method was used for loading of the model drug Dox into the hybrid MCM-41/AA-PnVCL particles. The particles were mixed with Dox in a weight ratio of 1:1 in 10 mL water on a magnetic stirrer for 2 h at 40°C temperature. Then, they were allowed to cool to room temperature. After the incubation, the samples were centrifuged at 14000 rpm for 20 min, washed three times with ethanol and dried under vacuum for 24 hours. Quantitative loading of Dox was determined by analyzing the obtained supernatant by UV-Vis absorption at 480 nm and was calculated by the formula:

$$\text{Drug loading efficiency (\%)} = \frac{A-B}{A} \times 100, \quad (1)$$

where A is the total weight of Dox used for the drug loading procedure, and B is the weight of Dox which is present in the supernatant.

4.3.8. In Vitro Drug Release Study

The prepared MCM-41/AA-PnVCL nanoparticles loaded with Dox were placed in a dialysis bag (MWCO: 6–8 kDa, Spectra/Por®) with phosphate buffer solution (PBS) (pH 4.0 and pH 7.4) and were immersed in buffered medium with the corresponding pH. Drug release was studied using an incubator shaker at 25°, 37° and 40°C respectively. Aliquots were withdrawn, analyzed by UV-vis spectroscopy at λmax= 480 nm and replaced with fresh medium at predetermined time points. A control experiment was conducted with free Dox to confirm that the selected dialysis membrane ensured unrestricted diffusion of the released drug. The highest drug concentration in the dialysate was below 10% of the drug's aqueous solubility, which is a prerequisite for "sink" conditions. The release study was performed in triplicates. Dox released amount was calculated based on a previously obtained calibration curve in the corresponding PBS medium. One-way ANOVA was used to determine the significance of the differences in the released amount. A significant level was set as $p<0.05$.

4.3.9. Haemolysis Assay

The haemolytic potential of the test substances was evaluated following the protocol described by Evans et al. 2013 [50]. Blood samples from healthy volunteers were obtained from a certified clinical laboratory. The experimental procedures were approved by the Institutional Ethics Committee (KENIMUS) at the Medical University, Sofia, Bulgaria and conducted according to the relevant protocols. The erythrocytes were separated from the blood by repeated centrifugation in 0.9% NaCl buffer. Then the blood cells were resuspended in phosphate buffer (pH 7.4). The test substances (at the appropriate concentrations), 20% Triton X-100 (used as a positive control group) and phosphate buffer (used as a negative control group) were pipetted into 96-well plates and the erythrocyte suspension in phosphate buffer was added to them. Thus, the plates were incubated for one hour at 37°C, then centrifuged for 5 min at 500 x g. The supernatant was moved to new 96-well plates, on which hemoglobin absorbance was measured at 430 nm in a Synergy 2 plate reader (BioTek Instruments, Inc, Highland Park, Winooski, USA). The results obtained were presented as the

percentage of hemolysis relative to the hemoglobin absorbance values in the positive controls, haemoglobin absorbance of negative controls was accepted as zero haemolysis. The substances that cause haemolysis below 5 % (the acceptable haemolytic threshold is 5% according to ISO 10993-5) were considered for biocompatible [51,52].

4.3.10. Statistical Analysis

Statistical analysis was performed by one-way ANOVA followed by a Dunnett post-hoc test. Statistical evaluation was performed using the GraphPad 6 software. Differences were accepted to be significant when $p<0.001$. All statistical analysis was carried out on Graph Pad 6 software. Results are expressed as a mean ± SD (n=6) for 3 independent experiments.

Author Contributions: Conceptualization, Ch.V. and M.S.; methodology, T.P., D.Tz., D.St. V.Tz., Iv.S., St.Tz and D.K.; software, D.St, D.Tz, Iv.S.; formal analysis, D.Tz, B.Tz. investigation, Iv.Iv.; resources, Ch.V.; data curation, Iv.Iv.; writing—original draft preparation, Ch.V. and M.S.; writing—review and editing, D.St., V.Tz, Ch.V. and M.S.; visualization, Iv.S., D.K, Ch.V. and M.S.; supervision, St.Tz., V.Tz and B.Tz; project administration, St.Tz. and Ch.V.; funding acquisition, St.Tz. and Ch.V.; All authors have read and agreed to the published version of the manuscript.

Funding: Iv.Iv. and St.Tz. acknowledge the financial support of Medical University-Pleven, Commission for Financing Research Projects, with financing project 9/2021.

Ch.V.: M.S., T.P., B.Tz. thank the funding provided by the European Union—NextGenerationEU, through the NationalRecovery and Resilience Plan of the Republic of Bulgaria, project No. BG-RRP-2.004-0004-C01.

Conflicts of Interest: The authors declare no conflict of interest.

Data Availability Statement: Data is available from the authors (see given emails).

References

1. Bukowski, K.; Kciuk, M.; Kontek, R. Mechanisms of Multidrug Resistance in Cancer Chemotherapy. *Int. J. Mol. Sci.* **2020**, *21*, 3233, doi:10.3390/ijms21093233.
2. Liu, Y.-Q.; Wang, X.-L.; He, D.-H.; Cheng, Y.-X. Protection against Chemotherapy- and Radiotherapy-Induced Side Effects: A Review Based on the Mechanisms and Therapeutic Opportunities of Phytochemicals. *Phytomedicine* **2021**, *80*, 153402, doi:10.1016/j.phymed.2020.153402.
3. Niu, G.; Cogburn, B.; Hughes, J. Preparation and Characterization of Doxorubicin Liposomes. In *Cancer Nanotechnology: Methods and Protocols*; Grobmyer, S.R., Moudgil, B.M., Eds.; Methods in Molecular Biology; Humana Press: Totowa, NJ, 2010; pp. 211–219 ISBN 978-1-60761-609-2.
4. Mal, A.; Prabhuraj, R.S.; Malhotra, R.; Valvi, S.K.; Ingle, A.; Srivastava, R.; De, A.; Bandyopadhyaya, R. PH-Responsive Sustained Delivery of Doxorubicin Using Aminated and PEGylated Mesoporous Silica Nanoparticles Leads to Enhanced Antitumor Efficacy in Pre-Clinical Orthotopic Breast Cancer Model. *J. Drug Deliv. Sci. Technol.* **2022**, *77*, 103800, doi:10.1016/j.jddst.2022.103800.
5. Moraes, S.; Marinho, A.; Lima, S.; Granja, A.; Araújo, J.P.; Reis, S.; Sousa, C.T.; Nunes, C. Targeted Nanostructured Lipid Carriers for Doxorubicin Oral Delivery. *Int. J. Pharm.* **2021**, *592*, 120029, doi:10.1016/j.ijpharm.2020.120029.
6. Valencia-Lazcano, A.A.; Hassan, D.; Pourmadadi, M.; shamsabadipour, A.; Behzadmehr, R.; Rahdar, A.; Medina, D.I.; Díez-Pascual, A.M. 5-Fluorouracil Nano-Delivery Systems as a Cutting-Edge for Cancer Therapy. *Eur. J. Med. Chem.* **2023**, *246*, 114995, doi:10.1016/j.ejmech.2022.114995.
7. Shao, D.; Gao, Q.; Sheng, Y.; Li, S.; Kong, Y. Construction of a Dual-Responsive Dual-Drug Delivery Platform Based on the Hybrids of Mesoporous Silica, Sodium Hyaluronate, Chitosan and Oxidized Sodium Carboxymethyl Cellulose. *Int. J. Biol. Macromol.* **2022**, *202*, 37–45, doi:10.1016/j.ijbiomac.2022.01.033.
8. Wei, G.; Wang, Y.; Yang, G.; Wang, Y.; Ju, R. Recent Progress in Nanomedicine for Enhanced Cancer Chemotherapy. *Theranostics* **2021**, *11*, 6370–6392, doi:10.7150/thno.57828.
9. Nawaz, A.; Ullah, S.; Alnuwaiser, M.A.; Rehman, F.U.; Selim, S.; Al Jaouni, S.K.; Farid, A. Formulation and Evaluation of Chitosan-Gelatin Thermosensitive Hydrogels Containing 5FU-Alginate Nanoparticles for Skin Delivery. *Gels* **2022**, *8*, doi:10.3390/gels8090537.
10. Slavkova, M.; Tzankov, B.; Popova, T.; Voycheva, C. Gel Formulations for Topical Treatment of Skin Cancer: A Review. *Gels* **2023**, *9*, 352, doi:10.3390/gels9050352.

11. Qureshi, D.; Nayak, S.K.; Maji, S.; Anis, A.; Kim, D.; Pal, K. Environment Sensitive Hydrogels for Drug Delivery Applications. *Eur. Polym. J.* **2019**, *120*, 109220, doi:10.1016/j.eurpolymj.2019.109220.
12. Li, L.; Scheiger, J.M.; Levkin, P.A. Design and Applications of Photoresponsive Hydrogels. *Adv. Mater.* **2019**, *31*, 1807333, doi:10.1002/adma.201807333.
13. Arneth, B. Tumor Microenvironment. *Medicina (Mex.)* **2020**, *56*, 15, doi:10.3390/medicina56010015.
14. Yu, Y.; Cheng, Y.; Tong, J.; Zhang, L.; Wei, Y.; Tian, M. Recent Advances in Thermo-Sensitive Hydrogels for Drug Delivery. *J. Mater. Chem. B* **2021**, *9*, 2979–2992, doi:10.1039/D0TB02877K.
15. Thananukul, K.; Kaewsaneha, C.; Opaprakasit, P.; Lebaz, N.; Errachid, A.; Elaissari, A. Smart Gating Porous Particles as New Carriers for Drug Delivery. *Adv. Drug Deliv. Rev.* **2021**, *174*, 425–446, doi:10.1016/j.addr.2021.04.023.
16. Bashir, S.; Hina, M.; Iqbal, J.; Rajpar, A.H.; Mujtaba, M.A.; Alghamdi, N.A.; Wageh, S.; Ramesh, K.; Ramesh, S. Fundamental Concepts of Hydrogels: Synthesis, Properties, and Their Applications. *Polymers* **2020**, *12*, 2702, doi:10.3390/polym12112702.
17. Raghuwanshi, V.S.; Garnier, G. Characterisation of Hydrogels: Linking the Nano to the Microscale. *Adv. Colloid Interface Sci.* **2019**, *274*, 102044, doi:10.1016/j.cis.2019.102044.
18. Zhang, Z.; Wang, S.; Waterhouse, G.I.N.; Zhang, Q.; Li, L. Poly(N-Isopropylacrylamide)/Mesoporous Silica Thermosensitive Composite Hydrogels for Drug Loading and Release. *J. Appl. Polym. Sci.* **2020**, *137*, 48391, doi:10.1002/app.48391.
19. Rout, S.R.; Gowtham, K.; Sheikh, A.; Parvez, S.; Dandela, R.; Kesharwani, P. Chapter 15 - Recent Advances and Future Prospective of Hybrid Drug Delivery Systems. In *Hybrid Nanomaterials for Drug Delivery*; Kesharwani, P., Jain, N.K., Eds.; Woodhead Publishing Series in Biomaterials; Woodhead Publishing, 2022; pp. 357–374 ISBN 978-0-323-85754-3.
20. Zhang, M.; Qiao, X.; Han, W.; Jiang, T.; Liu, F.; Zhao, X. Alginate-Chitosan Oligosaccharide-ZnO Composite Hydrogel for Accelerating Wound Healing. *Carbohydr. Polym.* **2021**, *266*, 118100, doi:10.1016/j.carbpol.2021.118100.
21. Mamidi, N.; Delgadillo, R.M.V. Design, Fabrication and Drug Release Potential of Dual Stimuli-Responsive Composite Hydrogel Nanoparticle Interfaces. *Colloids Surf. B Biointerfaces* **2021**, *204*, 111819, doi:10.1016/j.colsurfb.2021.111819.
22. Popescu, I.; Constantin, M.; Solcan, G.; Ichim, D.L.; Rata, D.M.; Horodincu, L.; Solcan, C. Composite Hydrogels with Embedded Silver Nanoparticles and Ibuprofen as Wound Dressing. *Gels* **2023**, *9*, 654, doi:10.3390/gels9080654.
23. Zhang, Z.; Ji, Y.; Lin, C.; Tao, L. Thermosensitive Hydrogel-Functionalized Gold Nanorod/Mesoporous MnO2 Nanoparticles for Tumor Cell-Triggered Drug Delivery. *Mater. Sci. Eng. C* **2021**, *131*, 112504, doi:10.1016/j.msec.2021.112504.
24. Liu, C.-M.; Chen, G.-B.; Chen, H.-H.; Zhang, J.-B.; Li, H.-Z.; Sheng, M.-X.; Weng, W.-B.; Guo, S.-M. Cancer Cell Membrane-Cloaked Mesoporous Silica Nanoparticles with a PH-Sensitive Gatekeeper for Cancer Treatment. *Colloids Surf. B Biointerfaces* **2019**, *175*, 477–486, doi:10.1016/j.colsurfb.2018.12.038.
25. Bharti, C.; Nagaich, U.; Pal, A.K.; Gulati, N. Mesoporous Silica Nanoparticles in Target Drug Delivery System: A Review. *Int. J. Pharm. Investig.* **2015**, *5*, 124–133, doi:10.4103/2230-973X.160844.
26. Hu, X.; Hao, X.; Wu, Y.; Zhang, J.; Zhang, X.; Wang, P.C.; Zou, G.; Liang, X.-J. Multifunctional Hybrid Silica Nanoparticles for Controlled Doxorubicin Loading and Release with Thermal and PH Dual Response. *J. Mater. Chem. B* **2013**, *1*, 1109–1118, doi:10.1039/C2TB00223J.
27. Voycheva, C.; Popova, T.; Slavkova, M.; Tzankova, V.; Stefanova, D.; Tzankova, D.; Spassova, I.; Kovacheva, D.; Tzankov, B. Doxorubicin and Quercetin Double Loading in Modified MCM-41 Lowered Cardiotoxicity in H9c2 Cardioblast Cells In Vitro. *Bioengineering* **2023**, *10*, 637, doi:10.3390/bioengineering10060637.
28. Djayanti, K.; Maharjan, P.; Cho, K.H.; Jeong, S.; Kim, M.S.; Shin, M.C.; Min, K.A. Mesoporous Silica Nanoparticles as a Potential Nanoplatform: Therapeutic Applications and Considerations. *Int. J. Mol. Sci.* **2023**, *24*, doi:10.3390/ijms24076349.
29. Dumontel, B.; Conejo-Rodríguez, V.; Vallet-Regí, M.; Manzano, M. Natural Biopolymers as Smart Coating Materials of Mesoporous Silica Nanoparticles for Drug Delivery. *Pharmaceutics* **2023**, *15*, 447, doi:10.3390/pharmaceutics15020447.
30. Lomartire, S.; Gonçalves, A.M.M. Algal Phycocolloids: Bioactivities and Pharmaceutical Applications. *Mar. Drugs* **2023**, *21*, 384, doi:10.3390/md21070384.

31. Lee, W.-K.; Lim, Y.-Y.; Leow, A.T.-C.; Namasivayam, P.; Abdullah, J.O.; Ho, C.-L. Factors Affecting Yield and Gelling Properties of Agar. *J. Appl. Phycol.* **2017**, *29*, 1527–1540, doi:10.1007/s10811-016-1009-y.
32. Voycheva, C.; Slavkova, M.; Popova, T.; Tzankova, D.; Tosheva, A.; Aluani, D.; Tzankova, V.; Ivanova, I.; Tzankov, S.; Spassova, I.; et al. Synthesis and Characterization of PnVCL Grafted Agar with Potential Temperature-Sensitive Delivery of Doxorubicin. *J. Drug Deliv. Sci. Technol.* **2022**, *76*, 103725, doi:10.1016/j.jddst.2022.103725.
33. Alam Khan, S.; Jawaid Akhtar, M. Structural Modification and Strategies for the Enhanced Doxorubicin Drug Delivery. *Bioorganic Chem.* **2022**, *120*, 105599, doi:10.1016/j.bioorg.2022.105599.
34. Voycheva, C.; Slavkova, M.; Popova, T.; Tzankova, D.; Tosheva, A.; Aluani, D.; Tzankova, V.; Ivanova, I.; Tzankov, S.; Spassova, I.; et al. Synthesis and Characterization of PnVCL Grafted Agar with Potential Temperature-Sensitive Delivery of Doxorubicin. *J. Drug Deliv. Sci. Technol.* **2022**, *76*, 103725, doi:10.1016/j.jddst.2022.103725.
35. Takahashi, R.; Sato, S.; Sodesawa, T.; Kawakita, M.; Ogura, K. High Surface-Area Silica with Controlled Pore Size Prepared from Nanocomposite of Silica and Citric Acid. *J. Phys. Chem. B* **2000**, *104*, 12184–12191, doi:10.1021/jp002662g.
36. Horcajada, P.; Rámila, A.; Férey, G.; Vallet-Regí, M. Influence of Superficial Organic Modification of MCM-41 Matrices on Drug Delivery Rate. *Solid State Sci.* **2006**, *8*, 1243–1249, doi:10.1016/j.solidstatesciences.2006.04.016.
37. Lai, Y.-L.; Cheng, Y.-M.; Yen, S.-K. Doxorubicin - Chitosan - Hydroxyapatite Composite Coatings on Titanium Alloy for Localized Cancer Therapy. *Mater. Sci. Eng. C* **2019**, *104*, 109953, doi:10.1016/j.msec.2019.109953.
38. Hu, S.H.; Fang, R.H.; Chen, Y.W.; Liao, B.J.; Chen, I.W.; Chen, S.-Y. Photoresponsive Protein-Graphene-Protein Hybrid Capsules with Dual Targeted Heat-Triggered Drug Delivery Approach for Enhanced Tumor Therapy. *Adv. Funct. Mater.* **2014**, *24*, 4144–4155, doi:10.1002/adfm.201400080.
39. Galhano, J.; Marcelo, G.A.; Duarte, M.P.; Oliveira, E. Ofloxacin@Doxorubicin-Epirubicin Functionalized MCM-41 Mesoporous Silica-Based Nanocarriers as Synergistic Drug Delivery Tools for Cancer Related Bacterial Infections. *Bioorganic Chem.* **2022**, *118*, 105470, doi:10.1016/j.bioorg.2021.105470.
40. Miao, Y.; Feng, Y.; Bai, J.; Liu, Z.; Zhao, X. Optimized Mesoporous Silica Nanoparticle-Based Drug Delivery System with Removable Manganese Oxide Gatekeeper for Controlled Delivery of Doxorubicin. *J. Colloid Interface Sci.* **2021**, *592*, 227–236, doi:10.1016/j.jcis.2021.02.054.
41. Yan, J.; Xu, X.; Zhou, J.; Liu, C.; Zhang, L.; Wang, D.; Yang, F.; Zhang, H. Fabrication of a PH/Redox-Triggered Mesoporous Silica-Based Nanoparticle with Microfluidics for Anticancer Drugs Doxorubicin and Paclitaxel Codelivery. *ACS Appl. Bio Mater.* **2020**, *3*, 1216–1225, doi:10.1021/acsabm.9b01111.
42. Dasgupta, D.; Das, M.; Thakore, S.; Patel, A.; Kumar, S.; Seshadri, S. Development of a Controlled Sustainable Anticancer Drug Delivery Nanosystem Comprising Doxorubicin and Functionalized MCM-48. *J. Drug Deliv. Sci. Technol.* **2022**, *72*, 103419, doi:10.1016/j.jddst.2022.103419.
43. Knežević, N.Ž.; Trewyn, B.G.; Lin, V.S.-Y. Light- and PH-Responsive Release of Doxorubicin from a Mesoporous Silica-Based Nanocarrier. *Chem. Weinh. Bergstr. Ger.* **2011**, *17*, 3338–3342, doi:10.1002/chem.201002960.
44. Sturgeon, R.J.; Schulman, S.G. Electronic Absorption Spectra and Protolytic Equilibria of Doxorubicin: Direct Spectrophotometric Determination of Microconstants. *J. Pharm. Sci.* **1977**, *66*, 958–961, doi:10.1002/jps.2600660714.
45. Janssen, M.J.H.; Crommelin, D.J.A.; Storm, G.; Hulshoff, A. Doxorubicin Decomposition on Storage. Effect of PH, Type of Buffer and Liposome Encapsulation. *Int. J. Pharm.* **1985**, *23*, 1–11, doi:10.1016/0378-5173(85)90217-0.
46. Hakeem, A.; Zahid, F.; Zhan, G.; Yi, P.; Yang, H.; Gan, L.; Yang, X. Polyaspartic Acid-Anchored Mesoporous Silica Nanoparticles for PH-Responsive Doxorubicin Release. *Int. J. Nanomedicine* **2018**, *13*, 1029–1040, doi:10.2147/IJN.S146955.
47. Maghsoudi, M.; Abbasian, M.; Farhadi, K.; Mahmoodzadeh, F.; Ghorbani, M.; Hoseinzadeh, M. Mesoporous Si-MCM-41/Polymer as a PH-Responsive Drug Delivery System for Cancer Therapy. *ChemistrySelect* **2020**, *5*, 11901–11909, doi:10.1002/slct.202002071.
48. Saroj, S.; Rajput, S.J. Tailor-Made PH-Sensitive Polyacrylic Acid Functionalized Mesoporous Silica Nanoparticles for Efficient and Controlled Delivery of Anti-Cancer Drug Etoposide. *Drug Dev. Ind. Pharm.* **2018**, *44*, 1198–1211, doi:10.1080/03639045.2018.1438467.

49. Zhao, Y.; Sun, X.; Zhang, G.; Trewyn, B.G.; Slowing, I.I.; Lin, V.S.-Y. Interaction of Mesoporous Silica Nanoparticles with Human Red Blood Cell Membranes: Size and Surface Effects. *ACS Nano* **2011**, *5*, 1366–1375, doi:10.1021/nn103077k.
50. Evans, B.C.; Nelson, C.E.; Yu, S.S.; Beavers, K.R.; Kim, A.J.; Li, H.; Nelson, H.M.; Giorgio, T.D.; Duvall, C.L. Ex Vivo Red Blood Cell Hemolysis Assay for the Evaluation of PH-Responsive Endosomolytic Agents for Cytosolic Delivery of Biomacromolecular Drugs. *J. Vis. Exp. JoVE* **2013**, e50166, doi:10.3791/50166.
51. 14:00-17:00 ISO 10993-5:2009 Available online: https://www.iso.org/standard/36406.html (accessed on 14 June 2023).
52. Romero, A.A.; Alba, M.D.; Zhou, W.; Klinowski, J. Synthesis and Characterization of the Mesoporous Silicate Molecular Sieve MCM-48. *J. Phys. Chem. B* **1997**, *101*, 5294–5300, doi:10.1021/jp970077i.